applied optics

Highly sensitive temperature sensor using a Sagnac loop interferometer based on a side-hole photonic crystal fiber filled with metal

Erick Reyes-Vera,[1,2,*] Cristiano M. B. Cordeiro,[3] and Pedro Torres[4]

[1]Department of Electrical and Electronic Engineering, Universidad Nacional de Colombia, Sede Bogotá, 11001, Colombia
[2]Department of Electronic and Telecommunications Engineering, Instituto Tecnológico Metropolitano, Medellín, Antioquia 050034, Colombia
[3]Instituto de Física Gleb Wataghin, Universidade Estadual de Campinas-UNICAMP, Campinas, SP 13083-859, Brazil
[4]Escuela de Física, Universidad Nacional de Colombia, Sede Medellín 3840, Colombia
*Corresponding author: erickreyes@itm.edu.co

Received 29 September 2016; revised 25 November 2016; accepted 2 December 2016; posted 5 December 2016 (Doc. ID 276421); published 3 January 2017

A highly sensitive temperature sensor based on an all-fiber Sagnac loop interferometer combined with metal-filled side-hole photonic crystal fiber (PCF) is proposed and demonstrated. PCFs containing two side holes filled with metal offer a structure that can be modified to create a change in the birefringence of the fiber by the expansion of the filler metal. Bismuth and indium were used to examine the effect of filler metal on the temperature sensitivity of the fiber-optic temperature sensor. It was found from measurements that a very high temperature sensitivity of −9.0 nm/°C could be achieved with the indium-filled side-hole PCF. The experimental results are compared to numerical simulations with good agreement. It is shown that the high temperature sensitivity of the sensor is attributed to the fiber microstructure, which has a significant influence on the modulation of the birefringence caused by the expansion of the metal-filled holes.

OCIS codes: (060.2270) Fiber characterization; (060.2280) Fiber design and fabrication; (060.2310) Fiber optics; (060.2370) Fiber optics sensors; (060.2400) Fiber properties; (120.5790) Sagnac effect.

https://doi.org/10.1364/AO.56.000156

1. INTRODUCTION

In the past two decades, fiber-optic sensors have had a major impact on various industry sectors, due to the advantages offered over traditional technologies, because they are highly compact, immune to electromagnetic noise, capable of remote sensing, and can be multiplexed. Currently, fiber-optic sensors are implemented in the measurement and monitoring of various physical variables such as pressure, displacement, temperature, refractive index, strain, etc. [1–7], with temperature sensors being the most studied and applied in recent years in the field of monitoring processes. Fiber gratings—fiber Bragg gratings (FBGs) [8,9] and long-period fiber gratings (LPGs) [10]—conventional high-birefringence (HiBi) optical fibers [11–14], waist-enlarged fusion bitaper [15], liquid-sealed tapered fibers [16], filled side-hole fibers [17–20], and filled photonic crystal fibers (PCFs) [21–24] have especially attracted great interest in temperature-sensing applications. Temperature sensors based on standard fibers have several drawbacks, mainly due to their low temperature sensitivity and a high sensitivity to bending and polarization [19]. For this reason, in recent years a variety of temperature sensors based on HiBi fibers have been reported, which have provided increased temperature sensitivity and robust characteristics on bending and polarization. Sensing solutions integrating a relatively short length of HiBi fiber in a Sagnac loop interferometer (SLI)—also known as fiber loop mirror (FLM)—are of great interest for temperature measurement. This interferometer consists of an optical coupler in which the 3 dB coupler splits the input light into two beams of clockwise and counterclockwise propagation. Each of the resultant beams is decomposed into two orthogonal modes after it travels through the HiBi fiber. The counterpropagating beams recombine at the optical coupler and exhibit interference according to the phase difference introduced to the two orthogonal-guided modes. It depends only on the fiber birefringence and length, being independent of the remaining ring extension. Utilizing conventional HiBi fibers, temperature sensors based on SLIs have been reported and have a sensitivity of ≈0.94 nm/°C, which is ≈94 times higher than those reported for FBGs [12]. However, the SLI sensor is usually quite long (≈72 cm) due to the limited birefringence of conventional HiBi fibers, which is not convenient for practical use. Side-hole conventional fibers offer a structure that can be modified to

create a change in the birefringence of the fiber by varying the mechanical stress in the fiber through properties of the filling material, such as metals or liquids that undergo a thermodynamic phase transition [17–20,25]. For example, a SLI temperature sensor based on 20-cm-long side-hole conventional fiber filled with indium (In) [18] has been presented by Kim *et al.*, achieving a high sensitivity of –6.3 nm/°C in the temperature range 27°C–115°C. Another recently explored option consists of using PCFs in which some or all holes of the fiber microstructure are filled with functional liquids such as alcohol [21], crystal liquids [22], polymer materials with a high thermo-optic coefficient [23], or index-matching fluids [24]. In a temperature sensor made by inserting a 6.1-cm alcohol-filled HiBi-PCF into a SLI [21], it was found that the sensing device could have the high sensitivity of 6.6 nm/°C, which is 7 times higher than that of the SLI made of a conventional HiBi fiber.

Thermo-optic mismatch between the two arms of all-fiber Mach–Zehnder interferometers (MZIs) has also been used as a temperature-sensing method. The much higher temperature sensitivity of 16.49 nm/°C has been experimentally demonstrated in a 4.1-cm-long modal MZI made by filling the index-matching fluid into one air hole next to the core of a solid-core PCF [26]. Although the temperature sensitivity could be significantly improved over those of the SLI sensors, the interference property in the modal MZI strongly relies on the coupling characteristics between the fundamental and higher-order modes of the fiber; thus the device performances, such as temperature range and sensitivity, are considerably affected by the mode-coupling conditions [23].

This work addresses the potential use of alternative temperature-sensing methods employing metal-filled side-hole PCFs. PCFs containing two side holes filled with metal offer a structure that can be modified to create a change in the birefringence by the expansion of the metal-filled holes. Recently, we studied the birefringence optical properties of side-hole PCFs filled with In by using the crossed polarizer low-coherence interferometric method [27,28]. We demonstrated that the fiber structure and the confinement factor of the fundamental mode significantly influence the temperature sensitivity of the birefringence.

In this paper, we propose and demonstrate a high-sensitivity temperature sensor by inserting a short metal-filled side-hole PCF into an SLI. Because of the temperature sensitivity of the fiber birefringence, an extremely high temperature sensitivity can be realized by measuring the wavelength shift of the resonant dips of the metal-filled side-hole PCF SLI. Here, the impact of different filler metals on the temperature sensitivity of the metal-filled side-hole PCF SLI sensor is also investigated. Bismuth (Bi), with a small expansion coefficient ($\alpha \approx 13.2 \times 10^{-3}$/K), and In, with a large expansion coefficient ($\alpha \approx 32.1 \times 10^{-3}$/K), were used in this investigation. As a result, the very large wavelength shift sensitivity, –9.0 nm/°C, was found in the SLI based on the In-filled side-hole PCF, and it is larger than that of the most sensitive SLI sensor reported so far, –7.38 nm/°C [19]. Numerical simulations were also performed for comparison with the experimental results, revealing that the fiber microstructure significantly influences the temperature sensitivity of the sensor.

2. SENSOR FABRICATION AND MEASUREMENT PRINCIPLE

Figure 1(a) shows the cross section of the fiber used in this study. The diameter of the fiber and width of the lateral holes were 170 μm and ~23 μm, respectively; in this sample, 15 μm separates the lateral holes from the edges of the core. The microstructure consists of five rings of air holes with a diameter of 1.05 μm and average pitch of 2.4 μm. The central solid core is 2.6 μm in diameter. The molten filler metals, at ~30°C higher than their melting temperatures, were injected into the holes of the fiber by the aid of compressed air at 3 bars, then self-cooled with the chamber turned off and closed [27,28]. Figures 1(b)–1(c) show images of the PCF with the side holes filled with Bi and In, respectively. As in our previous work [29], the two metals used in this study were well-incorporated by fully filling the side holes of the PCF to introduce the large thermal mismatch with silica glass ($\alpha = 5.5 \times 10^{-7}$/K) used as the fiber material. It is noted that the melting temperatures of In and Bi are 156.6°C and 270°C, respectively [30]. Note that the maximum operating temperature of this type of sensor is limited by the melting point of filler metals. When the metal is completely melted, only a minor temperature dependence remains, since the radial stress from the metal in the holes is relaxed [20].

The schematic structure of the metal-filled side-hole PCF SLI temperature sensor is presented in Fig. 1(d). The fiber loop was composed of the 3-dB optical fiber coupler made by the conventional single-mode fiber, the 22-cm-long metal-filled side-hole PCF, which was fusion-spliced to the arm of the fiber coupler, and a polarization controller. Both ends of the metal-filled PCF were free from metal to allow for convenient low-loss splicing. For each PCF sample, a length of 8 cm was heated in the temperature range 22°C–71°C by use of the heating system based on a semiconductor Peltier cooler. Owing to the thermal

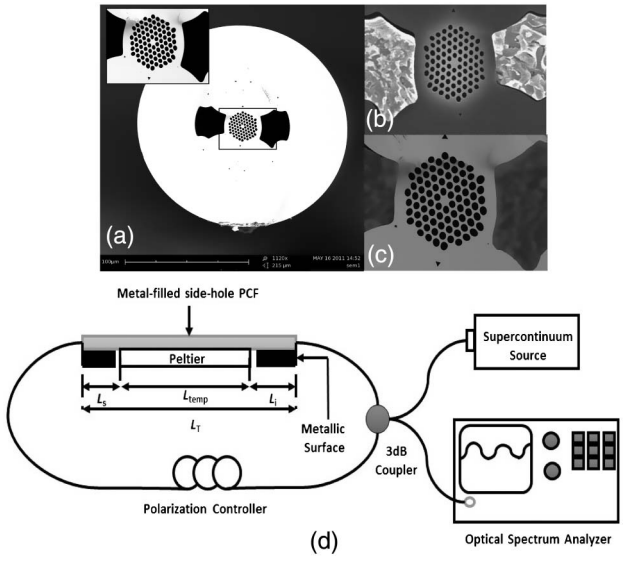

Fig. 1. Scanning electron microscope (SEM) images of the cross section of the side-hole PCF used in this study with different filler metals: (a) unfilled, (b) Bi, and (c) In, respectively. (d) Experimental setup of the SLI temperature sensor based on metal-filled side-hole PCF.

conductivity of metal inserted into the PCF, longitudinal heat transfer is expected in the fiber at the edges of the Peltier cooler; thus the fiber regions labeled L_i and L_s in Fig. 1(d) were maintained in thermal contact with metallic surfaces through a thermally conductive compound to maintain its temperature close to room temperature. Therefore, the fiber length over which the temperature decrease from Peltier temperature to room temperature was very short [29]. To improve the accuracy of the measurements, the interferogram on the output spectra was recorded over a large range of wavelengths by illuminating the test fiber with a supercontinuum source while recording the output spectrum using an optical spectrum analyzer (Yokogawa, AQ-6319). The polarizer control was used to maximize the visibility in the transmission spectra of the SLI.

As shown in Fig. 1(d), the directional coupler separates the input signal into two counterpropagating waves that subsequently recombine at the coupler after propagating around the loop. These two waves produce an optical path difference after transmitting through the metal-filled side-hole PCF because of its birefringence. Therefore, the transmission of the SLI temperature sensor is given by the periodic form

$$\psi = (1 - \cos \varphi_t)/2, \tag{1}$$

where φ_t is the birefringence-induced phase difference between the principal polarization modes that propagate in the PCF and is expressed by $2\pi\Delta n_g L_T/\lambda$. Here, λ is the wavelength of the propagating light, Δn_g is the group birefringence of the metal-filled side-hole PCF, and L_T is the length of the metal-filled side-hole PCF [see Fig. 1(d)]. The transmission dip wavelengths are the resonant wavelengths satisfying $2\pi\Delta n_g L_T/\lambda_{\text{dip}} = 2m\pi$, where m is any integer. Thus, the resonant dip wavelengths can be described as $\lambda_{\text{dip}} = \Delta n_g L_T/m$. Therefore, the wavelength spacing between transmission dips can be expressed as

$$\Delta\lambda = \frac{\lambda^2}{\Delta n_g L_T}; \tag{2}$$

thus, $\varphi_t = 2\pi\lambda_{\text{dip}}/\Delta\lambda$.

The sum of the phase differences arising at each of the segmented fiber regions gives the phase difference φ_t as follows:

$$\varphi_t = \frac{2\pi\Delta n_g L_T}{\lambda} = \frac{2\pi\lambda_{\text{dip}}}{\Delta\lambda} = \frac{2\pi(\Delta n_{g,\text{temp}} L_{\text{temp}} + \Delta n_{g,0} L_0)}{\lambda}; \tag{3}$$

thus,

$$\frac{\lambda_{\text{dip}}}{\Delta\lambda} = \frac{\Delta n_{g,\text{temp}} L_{\text{temp}} + \Delta n_{g,0} L_0}{\lambda}, \tag{4}$$

where $L_0 = L_i + L_s$ [see Fig. 1(d)]. Here, $\Delta n_{g,\text{temp}} L_{\text{temp}}$ is the product of the group birefringence and length for the fiber region exposed to the temperature (T) change inside the Peltier cooler, and $\Delta n_{g,0} L_0$ is the product of the group birefringence and length for the fiber outside the Peltier cooler at room temperature. In the equation, Δn_g indicates the effective fiber birefringence that manifests the overall property of the metal-filled side-hole PCF. Since $\Delta n_{g,0} L_0$ is constant with respect to the temperature variation, the temperature-induced wavelength shift sensitivity of the interference fringe is derived as

$$\frac{d\lambda_{\text{dip}}}{dT} = \frac{\Delta\lambda}{\lambda}\left[\frac{d\Delta n_{g,\text{temp}}}{dT} L_{\text{temp}} + \Delta n_{g,\text{temp}} \frac{dL_{\text{temp}}}{dT}\right]. \tag{5}$$

The contribution from the modulation of the fiber birefringence induced by the expansion of the metal would be much larger than that from the variation of the fiber length due to thermal expansion [28], and therefore, the equation can be further simplified by neglecting the second term in Eq. (5). Thus, the final form of the wavelength sensitivity for the sensor device based on the metal-filled side-hole PCF SLI is given by

$$\frac{d\lambda_{\text{dip}}}{dT} \approx \frac{\Delta\lambda}{\lambda}\left[\frac{d\Delta n_{g,\text{temp}}}{dT} L_{\text{temp}}\right]. \tag{6}$$

In addition, the sensitivity for the case that the whole length of the metal-filled side-hole PCF is exposed to the temperature variation can be estimated by multiplying with the term L_T/L_{temp} [23], as follows:

$$\left.\frac{d\lambda_{\text{dip}}}{dT}\right|_{L_T} \approx \left.\frac{d\lambda_{\text{dip}}}{dT}\right|_{L_{\text{temp}}} \times \frac{L_T}{L_{\text{temp}}}. \tag{7}$$

3. RESULTS AND DISCUSSION

Figure 2 shows the recorded interferograms on the output spectra of the SLI sensor using the side-hole PCF filled with Bi and In at room temperature (the Peltier cooler is off), ~22°C. For comparison, this figure includes the interferogram on the output spectrum of the SLI using the unfilled PCF. As we can see, the spectral ripple period decreases with the incorporation of the metals. This behavior is caused by the difference between the thermal expansion coefficients for the fiber and the filler metal. Also, each metal generates different permanent stress field when cooled down to room temperature, which explains the difference among them [17]. The relatively large insertion loss of the three devices may be created in the splicing process.

The temperature sensitivity of the metal-filled side-hole PCF SLI sensor was examined by monitoring the interferograms on the output spectra at different temperatures. Figure 3 shows the results for the metal-filled side-hole PCF

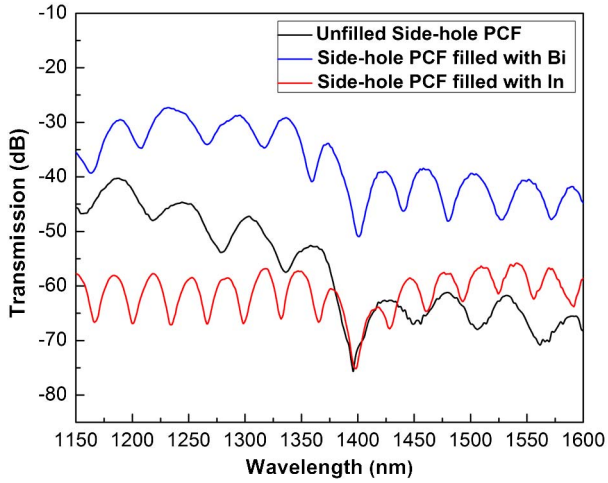

Fig. 2. Transmission spectra of the SLI based on side-hole PCF without and with metal at room temperature (~22°C). The spectra were shifted vertically for clarity.

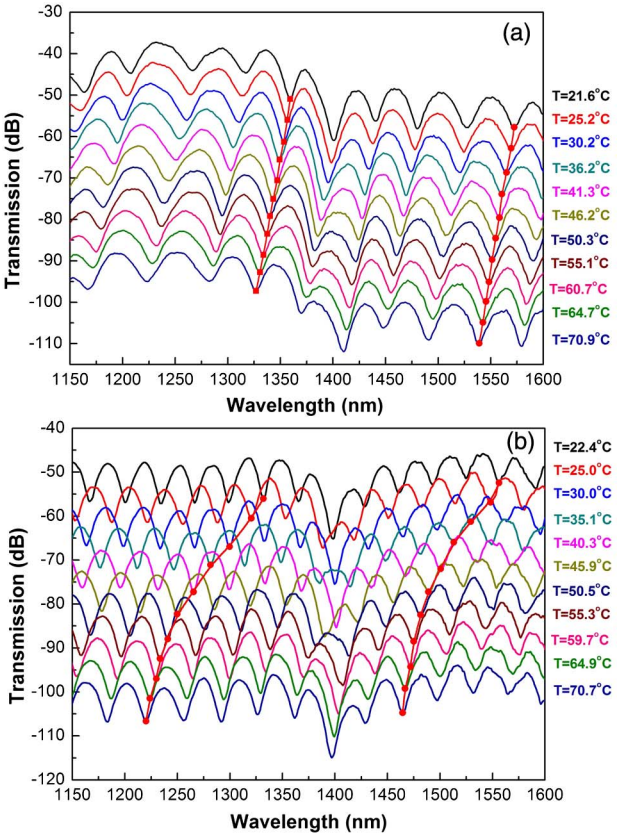

Fig. 3. Transmission spectra of the SLI based on side-hole PCF filled with (a) Bi; (b) In. The spectra were shifted vertically for clarity. The red line shows the wavelength shift.

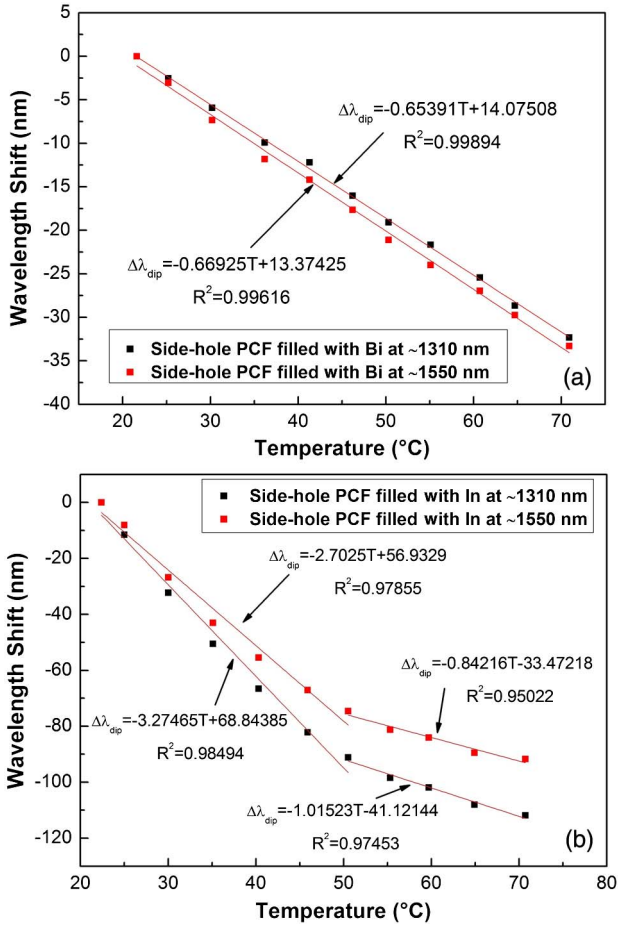

Fig. 4. Wavelength shift of the interference fringe of the SLI temperature sensor based on metal-filled side-hole PCF with $L_T \sim 22$ cm and $L_{\text{temp}} \sim 8$ cm. (a) PCF filled with Bi; (b) PCF filled with In.

SLI device for the wavelength range from 1150 to 1600 nm. As we can see, in both metals the interference fringe shifted to shorter wavelengths as the temperature increased, and this agrees with previous reports in side-hole conventional fibers filled with metal [17,18]. The magnitudes of the wavelength shift of the interference fringe versus temperature are presented in Fig. 4. In the case of the PCF filled with Bi, the wavelength shift shows good linearity in the measurement range of 21.6°C–70.9°C. The temperature sensitivities of the sensor were estimated to be −0.654 nm/°C ($R^2 \sim 0.998$) and −0.670 nm/°C ($R^2 \sim 0.996$) for interference dips near the wavelengths 1350 nm and 1550 nm, respectively, which are ∼3.5 times larger than the wavelength shift sensitivity in SLIs using side-hole conventional fiber filled with Bi at 1310 nm [17], where R^2 denotes the regression coefficients of linear fitting. On the other side, in the PCF filled with In, it is clear that there are two regions of operation. During the initial temperature increase from 22.4°C to 46°C, the interference fringe monotonously shifted to the shorter wavelength at the rate of −3.275 nm/°C ($R^2 \sim 0.985$) and −2.702 nm/°C ($R^2 \sim 0.979$) for interference dips near the wavelengths 1310 nm and 1550 nm, respectively, which is ∼5 times larger than the wavelength shift sensitivity of the previous case with Bi and same order of the sensitivity reported in SLIs using side-hole conventional fiber filled with In [18]. In the second region of operation, from 50.5°C to 70.7°C, the wavelength shift sensitivity changes, which is estimated to be −1.015 nm/°C ($R^2 \sim 0.975$) and −0.842 nm/°C ($R^2 \sim 0.950$) for interference dips near the wavelengths 1310 nm and 1550 nm, respectively. As already explained, the modulation of the fiber birefringence is accomplished through the stress field induced by the expansion of the metal-filled holes. Stress is increased between the holes of fiber microstructure due to the thermal load of the metal insertion process. In the case of the PCF filled with In, these stresses are channeled further in direction toward the core [28]. This explains the difference in the temperature sensibility between the fibers with two holes filled with Bi and In. From the measured sensitivities and Eq. (7), the sensitivities for the case of the whole length of the metal-filled side-hole PCF exposed to the temperature variation were estimated to be −1.80 nm/°C ($\lambda_{\text{dip}} = 1350$ nm) and −1.84 nm/°C ($\lambda_{\text{dip}} = 1550$ nm) in the whole temperature range for the PCF with Bi, −9.0 nm/°C ($\lambda_{\text{dip}} = 1310$ nm) and −7.43 nm/°C ($\lambda_{\text{dip}} = 1550$ nm) in the temperature range 22.4°C–46°C for the PCF with In, and −2.79 nm/°C ($\lambda_{\text{dip}} = 1310$ nm) and −2.32 nm/°C ($\lambda_{\text{dip}} = 1550$ nm) in the temperature range 50.5°C–70.7°C for the PCF with In.

The temperature can be measured from the fringe spacing itself because the fringe spacing as well as the wavelength shift

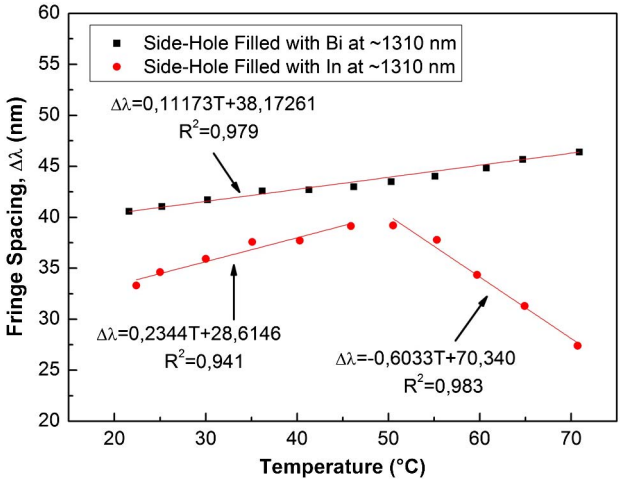

Fig. 5. Interference fringe spacing near 1310 nm of the SLI temperature sensor based on metal-filled side-hole PCF with $L_T = 22$ cm and $L_{\text{temp}} = 8$ cm.

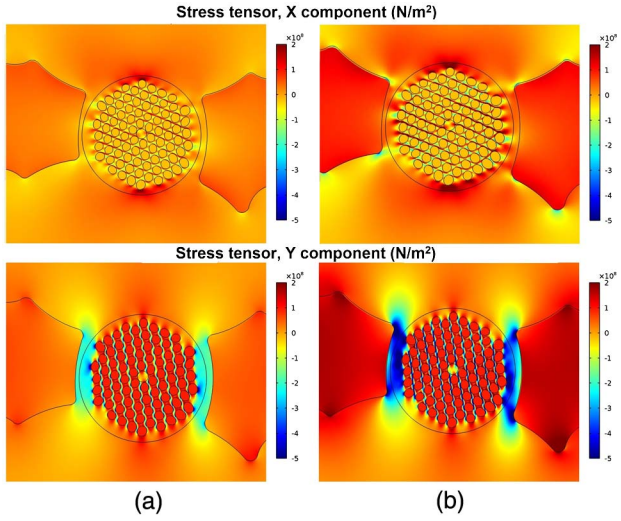

Fig. 6. Computed stress distributions along horizontal (x) and vertical (y) axes for the side-hole PCF filled with (a) Bi and (b) In at 45°C.

depends considerably on temperature; see Eqs. (2) and (6). As an example, Fig. 5 shows the fringe spacings of sensors near 1310 nm in the temperature range of ≈22°C–70°C. The temperature sensitivity of the fringe spacing with the increase of the temperature was estimated to be 0.112 nm/°C in the whole temperature range for the PCF with Bi, and 0.234 nm/°C and −0.603 nm/°C in the temperature ranges 22.4°C–46°C and 50.5°C–70.7°C, respectively, for the PCF with In. The results show that we can use this information as a reference signal to identify the traced fringe in the wavelength shift approach. In comparison to the wavelength-shift approach, this scheme has less sensitivity. However, it permits the application of interferometric signal demodulation for automated measurement [31].

To understand the optical properties of the sensor device, numerical simulations were developed. Our procedure consists of two steps. In the first step, 2D finite element method (FEM) simulations are developed by using COMSOL Multiphysics to determine the spectral dependence of the group birefringence $\Delta n_{g,\text{temp}}$ in the temperature range 22°C–70°C. For the simulations, the fiber geometry shown in Fig. 1 is used. Importantly, our technique couples the stress-induced changes to the refractive index on the fiber cross section, which are caused by the elasto-optical effect related to the interplay between the residual stress induced by the metal infiltration process and the stress induced by the expansion of the filler metal with the temperature, with the solution of the full vectorial wave equation for the electric field. The details of the method and material properties can be found in [28]. As an example, Fig. 6 compares the calculated stress distributions along the horizontal and vertical axes for the side-hole PCF filled with Bi and In at 45 °C. From this figure, it is clear that the magnitude and distribution of stress, especially in the fiber core, are governed by the distribution of the holes in the microstructure and depend strongly on the filler metal, which explains the difference in the temperature sensibility between the side-hole fibers filled with Bi and In. As already explained, the modulation of the fiber birefringence is accomplished through the stress field induced by the expansion of the metal-filled holes. A comprehensive study of the influence of the filler metal on the average values of the principal stresses near the fiber center with temperature, and consequently, on the birefringent optical properties of a metal-filled side-hole PCF, can be found in [29].

On the other side, birefringence results obtained from the first step for the two representative wavelengths are shown in Fig. 7. From these results, the dependence on the wavelength of the birefringence is clear, which is explained by the gradual expansion of the fundamental mode into the fiber microstructure. We can also see that for the case of the PCF filled with Bi, the group birefringence decreases almost linearly with the increasing temperature, while for the case of the PCF filled with In, the group birefringence presents anomalous behavior: the birefringence decreases in the temperature range 20°C–45°C, after which it increases.

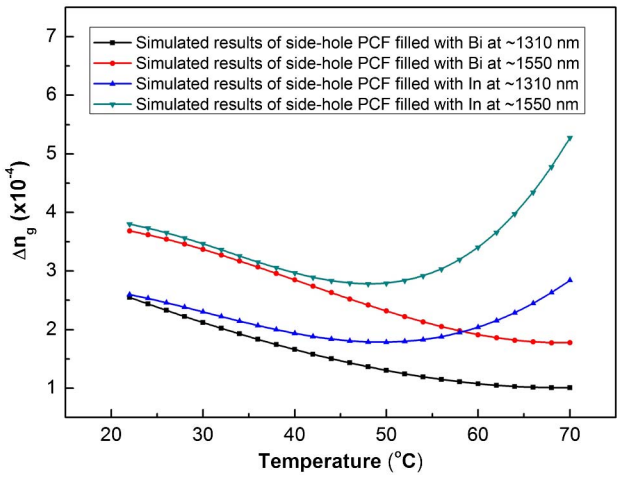

Fig. 7. Numerical results of group birefringence of the side-hole PCF filled with (a) Bi and (b) In as a function of the temperature for two representative wavelengths.

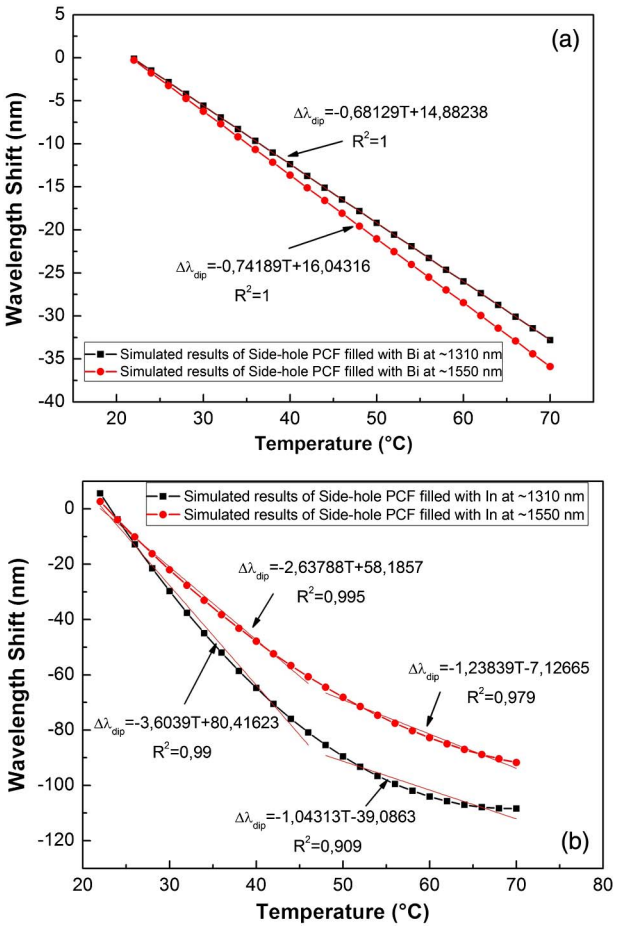

Fig. 8. Theoretical wavelength shift of the interference fringe of the SLI temperature sensor based on the side-hole PCF filled with (a) Bi and (b) In.

In the second step of our simulation procedure, the spectral dependence of the group birefringence of the previous step is used to derive the phase difference $\varphi_t(\lambda)$ by using Eq. (3) and the transmittance characteristic by using Eq. (1), as a function of temperature for the same sensor. Thus, the interferograms on the output spectra of the sensor device were obtained, and the interference dips can be examined. The magnitudes of the theoretical wavelength shift versus temperature are presented in Fig. 8. Note that our model describes the good linearity and the nonlinear behavior of the sensor device with Bi and In, respectively. In addition, the theoretical values of temperature sensitivity of the wavelength shift are in good agreement with the experimental results in Fig. 4. It is evident that our model successfully explains all the essential features of the metal-filled side-hole PCF SLI temperature sensor. Although the air-hole structure influences the birefringence generated by the expansion of the metal when subjected to temperature changes, it has been obtained by a high-sensitivity temperature sensor as compared to fiber-optic temperature sensors reported to date, as can be seen from Table 1, which summarizes the different optical fiber configurations (interferometric, SLI, mode coupling) with improved characteristics through the use of liquids or metals whose physical properties (birefringence, thermo-optical coefficient, thermal expansion) are highly dependent on temperature variations in order to achieve better temperature-sensor characteristics. To the knowledge of the authors, the temperature sensitivity of the sensor demonstrated in this study would be larger than the value −7.38 nm/°C of the most sensitive SLI sensor reported so far [19].

4. CONCLUSION

In summary, a highly temperature-sensitive all-fiber Sagnac loop interferometric sensor based on metal-filled side-hole

Table 1. Comparison of Recently Reported Fiber-Optic Temperature Sensors

Technique	Temperature Range	Temperature Sensitivity (S_T)	Length (L)	S_T/L	Reference
Fabry–Perot interferometric sensor using the difference of thermal expansion coefficient between fused silica and metallic materials	−79°C–70°C	14 pm/°C	1.2 μm	NA[a]	[32]
Alcohol-filled side-hole fiber	20°C–72°C	86.8 pm/°C	15 cm	0.0579 nm/(°C · cm)	[25]
Mach–Zehnder Interferometric sensor based on a waist-enlarged fusion Bi taper	25°C–400°C	0.07 nm/°C	7.5 mm	0.0933 nm/(°C · cm)	[15]
In fiber Michelson interferometer based on a thin-core fiber Bi taper	30°C–800°C	0.140 nm/°C	2 × 1.4 mm	0.5000 nm/(°C · cm)	[33]
Liquid-sealed S-tapered fiber	20°C–50°C	−1.403 nm/°C	10 mm	NA[a]	[16]
PANDA fiber end-face-type Sagnac Interferometer	40°C–60°C	−1.46 nm/°C	2 × 6 mm	−1.2083 nm/(°C · cm)	[34]
Selectively filled PCF SLI	25°C–42°C	2.58 nm/°C	11.7 cm	0.2205 nm/(°C · cm)	[35]
Droplet-like fiber circle	18°C–30°C	−3.102 nm/°C	10–20 cm	NA[a]	[36]
Selectively liquid crystal (LC)-filled PCF directional coupler circle	44°C–53°C	−3.90 nm/°C	1–10 cm	NA[a]	[22]
Alcohol-filled PCF	8°C–20°C 20°C–34°C	6.6 nm/°C 6.2 nm/°C	6.1 cm	1.0819 nm/(°C · cm) 1.0164 nm/(°C · cm)	[21]
In-filled side-hole conventional fiber end-face-type Sagnac Interferometer	18°C–86°C	−7.38 nm/°C	2 × 20 cm	−0.1845 nm/(°C · cm)	[19]
SLI sensor using In-filled side-hole PCF SLI sensor using Bi-filled side-hole PCF	22.4°C–46°C 21.6°C–70.7°C	−9.0 nm/°C −1.80 nm/°C	22 cm	−0.4091 nm/(°C · cm) −0.0818 nm/(°C · cm)	This work

[a]Abbreviation: NA, not applicable.

PCF was proposed, and its optical properties were experimentally and theoretically investigated. It was found from measurements that the temperature sensitivity of the sensor device was larger for the filler metal with the larger thermal expansion coefficient and the very high temperature sensitivity of −9.0 nm/°C could be achieved with the side-hole PCF filled with In. The high temperature sensitivity is attributed to the fiber microstructure, which has a significant influence on the modulation of the birefringence induced by the stress field caused by the expansion of the metal-filling holes.

Funding. Universidad Nacional de Colombia (UN) (225677, 32150); Instituto Tecnológico Metropolitano (ITM) (P15108); Fundação de Amparo à Pesquisa do Estado de São Paulo (FAPESP); Coordenação de Aperfeiçoamento de Pessoal de Nível Superior (CAPES); Financiadora de Estudos e Projetos (FINEP).

Acknowledgment. The authors thank Giancarlo Chesini, State University of Campinas, Brazil, for technical assistance with the metal-filling process.

REFERENCES

1. B. Lee, "Review of the present status of optical fiber sensors," Opt. Fiber Technol. **9**, 57–79 (2003).
2. B. Culshaw and A. Kersey, "Fiber-optic sensing: a historical perspective," J. Lightwave Technol. **26**, 1064–1078 (2008).
3. J. M. López-Higuera, L. Rodriguez Cobo, A. Quintela Incera, and A. Cobo, "Fiber optic sensors in structural health monitoring," J. Lightwave Technol. **29**, 587–608 (2011).
4. G. Wehrle, H. J. Kalinowski, P. I. Torres, and L. C. Guedes-Valente, "Fibre optic Bragg grating strain sensor used to monitor the respiratory spectrum," Proc. SPIE **4185**, 310–313 (2000).
5. Y. Wang, D. N. Wang, C. R. Liao, T. Hu, J. Guo, and H. Wei, "Temperature-insensitive refractive index sensing by use of micro Fabry–Perot cavity based on simplified hollow-core photonic crystal fiber," Opt. Lett. **38**, 269–271 (2013).
6. Y. Zou, X. Dong, G. Lin, and R. Adhami, "Wide range FBG displacement sensor based on twin-core fiber filter," J. Lightwave Technol. **30**, 337–343 (2012).
7. P. Torres, E. Reyes-Vera, A. Díez, and M. V. Andrés, "Two-core transversally chirped microstructured optical fiber refractive index sensor," Opt. Lett. **39**, 1593–1596 (2014).
8. A. D. Kersey, M. A. Davis, H. J. Patrick, M. LeBlan, K. P. Koo, C. G. Askins, M. A. Putnam, and E. Friebele, "Fiber grating sensors," J. Lightwave Technol. **15**, 1442–1463 (1997).
9. Y. Zou and X. Dong, "Demodulation of the FBG temperature sensor with the tunable twin-core fiber," Microwave Opt. Technol. Lett. **53**, 81–84 (2011).
10. V. Bhatia and A. M. Vengsarkar, "Optical fiber long-period grating sensors," Opt. Lett. **21**, 692–694 (1996).
11. A. N. Starodumov, L. A. Zenteno, D. Monzon, and E. De La Rosa, "Fiber Sagnac interferometer temperature sensor," Appl. Phys. Lett. **70**, 19–21 (1997).
12. Y. Liu, B. Liu, X. Feng, W. Zhang, G. Zhou, S. Yuan, G. Kai, and X. Dong, "High-birefringence fiber loop mirrors and their applications as sensors," Appl. Opt. **44**, 2382–2390 (2005).
13. O. Frazão, J. M. T. Baptista, and J. L. Santos, "Recent advances in high-birefringence fiber loop mirror sensors," Sensors **7**, 2970–2983 (2007).
14. X. Dong, H. Y. Tam, and P. Shum, "Temperature-insensitive strain sensor with polarization-maintaining photonic crystal fiber based Sagnac interferometer," Appl. Phys. Lett. **90**, 1511131 (2007).
15. Y. Geng, X. Li, X. Tan, Y. Deng, and Y. Yu, "High-sensitivity Mach–Zehnder interferometric temperature fiber sensor based on a waist-enlarged fusion bitaper," IEEE Sens. J. **11**, 2891–2894 (2011).
16. R. Yang, Y. S. Yu, Y. Xue, C. Chen, C. Wang, F. Zhu, B. L. Zhang, Q. D. Chen, and H. B. Sun, "A highly sensitive temperature sensor based on a liquid-sealed S-tapered fiber," IEEE Photon. Technol. Lett. **25**, 829–832 (2013).
17. S. H. Lee, B. H. Kim, and W. Han, "Effect of filler metals on the temperature sensitivity of side-hole fiber," Opt. Express **17**, 9712–9717 (2009).
18. B. H. Kim, S. H. Lee, A. Lin, C. Lee, J. Lee, and W. Han, "Large temperature sensitivity of Sagnac loop interferometer based on the birefringent holey fiber filled with metal indium," Opt. Express **17**, 1789–1794 (2009).
19. B. H. Kim, S. Lee, D. H. Son, T. Ahn, S. Kim, and W. Han, "Optical properties of the fiber-optic temperature sensor based on the side-hole fiber filled with indium," Appl. Opt. **52**, 666–673 (2013).
20. J. Jason, P. Rugeland, O. Tarasenko, W. Margulis, and H. Nilsson, "Temperature characteristics of the birefringence properties of filled side-hole fibers," Appl. Opt. **52**, 5208–5215 (2013).
21. W. Qian, C.-L. Zhao, S. He, X. Dong, S. Zhang, Z. Zhang, S. Jin, J. Guo, and H. Wei, "High-sensitivity temperature sensor based on an alcohol-filled photonic crystal fiber loop mirror," Opt. Lett. **36**, 1548–1550 (2011).
22. D. J. J. Hu, J. L. Lim, Y. Cui, K. Milenko, Y. Wang, P. P. Shum, and T. Wolinski, "Fabrication and characterization of a highly temperature sensitive device based on nematic liquid crystal-filled photonic crystal fiber," IEEE Photon. J. **4**, 1248–1255 (2012).
23. K. Naeem, B. H. Kim, B. Kim, and Y. Chung, "High-sensitivity temperature sensor based on a selectively-polymer-filled two-core photonic crystal fiber in-line interferometer," IEEE Sens. J. **15**, 3998–4003 (2015).
24. M. Yang, D. N. Wang, Y. Wang, and C. R. Liao, "Fiber in-line Mach–Zehnder interferometer constructed by selective infiltration of two air holes in photonic crystal fiber," Opt. Lett. **36**, 636–638 (2011).
25. Y. Xin, X. Dong, Q. Meng, F. Qi, and C.-L. Zhao, "Alcohol-filled side-hole fiber Sagnac interferometer for temperature measurement," Sens. Actuators A Phys. **193**, 182–185 (2013).
26. H. Liang, W. Zhang, H. Wang, P. Geng, S. Zhang, S. Gao, C. Yang, and J. Li, "Fiber in-line Mach–Zehnder interferometer based on near-elliptical core photonic crystal fiber for temperature and strain sensing," Opt. Lett. **38**, 4019–4022 (2013).
27. E. Reyes-Vera, G. Chesini, C. M. Cordeiro, and P. Torres, "Large temperature sensitivity of birefringent side-hole photonic crystal fiber filled with Indium," in *Workshop on Specialty Optical Fibers and their Applications* (Optical Society America, 2013), Vol. **1**, paper W3.16.
28. E. Reyes-Vera, N. D. Gómez-Cardona, G. Chesini, C. M. B. Cordeiro, and P. Torres, "Temperature sensibility of the birefringence properties in side-hole photonic crystal fiber filled with Indium," Appl. Phys. Lett. **105**, 201101 (2014).
29. E. Reyes-Vera and P. Torres, "Influence of filler metal on birefringent optical properties of PCF with integrated electrodes," J. Opt. **18**, 085804 (2016).
30. D. R. Lide, *CRC Handbook of Chemistry and Physics*, 1st ed. (CRC Press, 2005).
31. D. W. Kim, Y. Zhang, K. L. Cooper, and A. Wang, "In-fiber reflection mode interferometer based on a long-period grating for external refractive-index measurement," Appl. Opt. **44**, 5368–5373 (2005).
32. X. Li, S. Lin, J. Liang, Y. Zhang, H. Oigawa, and T. Ueda, "Fiber-optic temperature sensor based on difference of thermal expansion coefficient between fused silica and metallic materials," IEEE Photon. J. **4**, 155–162 (2012).
33. N. Zhao, H. Fu, M. Shao, X. Yan, H. Li, Q. Liu, H. Gao, Y. Liu, and X. Qiao, "High temperature probe sensor with high sensitivity based on Michelson interferometer," Opt. Commun. **343**, 131–134 (2015).
34. J. Zhang, X. Qiao, T. Guo, Y. Weng, R. Wang, Y. Ma, Q. Rong, M. Hu, and Z. Feng, "Highly sensitive temperature sensor using PANDA fiber Sagnac interferometer," J. Lightwave Technol. **29**, 3640–3644 (2011).
35. Y. Cui, P. P. Shum, D. J. J. Hu, G. Wang, G. Humbert, and X.-Q. Dinh, "Temperature sensor by using selectively filled photonic crystal fiber Sagnac interferometer," IEEE Photon. J. **4**, 1801–1808 (2012).
36. J. Xie, B. Xu, Y. Li, J. Kang, C. Shen, J. Wang, Y. Jin, H. Liu, K. Ni, X. Dong, C. Zhao, and S. Jin, "High-sensitivity temperature sensor based on a droplet-like fiber circle," Appl. Opt. **53**, 4085–4088 (2014).